A ML-Based Framework for Joint TOA/AOA Estimation of UWB Pulses in Dense Multipath Environments

Fang Shang, *Student Member, IEEE*, Benoit Champagne, *Senior Member, IEEE*, and Ioannis N. Psaromiligkos, *Member, IEEE*

***Abstract*—We present a joint estimator of the time of arrival (TOA) and angle of arrival (AOA) for impulse radio ultra-wideband (UWB) systems in which an antenna array is employed at the receiver. The proposed method consists of two steps: 1) preliminary estimation of the TOA and the average power delay profile (APDP) using energy-based threshold crossing and log-domain least-squares fitting, respectively; and 2) joint TOA refinement and AOA estimation by local 2-D maximization of a log-likelihood function (LLF) that employs the preliminary estimates from the first step. The derivation of the LLF relies on an original formulation in which the superposition of images from secondary paths is modeled as a Gaussian random process, whose second-order statistical properties are characterized by a wide-band space–time correlation function. In addition to the APDP, this function incorporates a special gating mechanism to represent the onset of the secondary paths, thereby leading to a novel form of the LLF. Closed-form expressions for the Cramer–Rao bound on the variance of the TOA and AOA estimators are also derived, which formally take into account pulse overlap through this gating mechanism. In simulation experiments based on multipath UWB channel models featuring both diffuse and directional image fields, our approach exhibits superior performance to that of a competing scheme from the recent literature.**

***Index Terms*—Ultrawideband (UWB), impulse radio, angle of arrival (AOA), time of arrival (TOA), average power delay profile (APDP), maximum-likelihood (ML) estimation.**

I. Introduction

LOCALIZATION of objects (including persons or animals) using impulse radio (IR) ultra wideband (UWB) technology has been gaining wide acceptance by industries and government agencies in recent years, especially within the contexts of radio frequency identification (RFID), wireless sensor networks (WSN) and wireless local area networks (WLAN) [1]–[6]. In active UWB localization, a battery powered low-cost transmitter attached to the object of interest, emits a coded sequence of very short electromagnetic impulses, with duration of the order of a nanosecond or less. One or more receivers with known positions are then employed to monitor the propagating pulses and extract relevant information about the object, including its identification and location. Due to the fine time resolution nature of IR-UWB signals, very accurate positioning of the source can be achieved in this way. With the reduction in manufacturing costs, sizes and energy consumptions of the UWB emitters, IR-UWB has been adopted widely for indoor localization, with numerous applications ranging from container positioning and inventory management, to mining safety and health-care.

Estimation of the time-of-arrival (TOA) of the transmitted pulses by three or more (non-collinear) receivers enables the localization of the desired source [7], [8]. Many approaches have been proposed for TOA estimation using IR-UWB signals, assuming time clock synchronization between the source and receiver. The conventional maximum likelihood (ML) TOA estimator employs a coherent processing structure at the receiver [9], [10], which typically operates at the Nyquist sampling rate and achieves very good accuracy. Alternatively, TOA estimation algorithms based on noncoherent energy detection (ED) receiver have been thoroughly investigated using sub-Nyquist sampling (see [11]). In the ED approach, the TOA is normally estimated as the threshold-crossing (TC) point of a time-localized energy measure, where the threshold depends on the statistics of the received signal and channel [12], [13]. However, radio noise is enhanced by the receiver at low signal-to-noise ratio (SNR), which will inevitably degrade the performance of the detector in a way that depends on the threshold (i.e., larger false alarm or missed detection probabilities). Other sub-Nyquist sampling methods include the transmitted-reference (TR) receiver [14], as well as ML-based estimators assuming various levels of *a priori* channel information [15]. In general, the accuracy of TOA estimation is sacrificed for the integrator's low time resolution, and a trade-off must be reached between estimation performance and implementation complexity. In [16] and [17], we propose a new sub-Nyquist approach for the joint estimation of the TOA and APDP, where the latter is modeled as a sum of exponentially decaying clusters. The combined use of this estimated APDP with the proposed ML-based TOA estimator (as well as other existing TOA estimators) leads to noticeable improvements in TOA estimation accuracy.

In theory, the number of required receivers for localization can be reduced if the angle-of-arrival (AOA) of the transmitted

Manuscript received April 7, 2013; revised September 12, 2013, January 24, 2014, and June 15, 2014; accepted July 10, 2014. Date of publication July 25, 2014; date of current version October 8, 2014. This work was supported in part by the Fonds Québécois de la Recherche sur la Nature et les Technologies. This paper was presented in part at the 2013 IEEE International Conference on Acoustics, Speech and Signal Processing (ICASSP), Vancouver, BC, Canada. The associate editor coordinating the review of this paper and approving it for publication was T. Zemen.

The authors are with the Department of Electrical and Computer Engineering, McGill University, Montreal, QC H3A 0E9, Canada (e-mail: fang.shang@mail.mcgill.ca; benoit.champagne@mcgill.ca; yannis@ece.mcgill.ca).

Color versions of one or more of the figures in this paper are available online at http://ieeexplore.ieee.org.

Digital Object Identifier 10.1109/TWC.2014.2343634

pulses can be estimated jointly with the TOAs [18]. In this case, each receiver must be equipped with an array of antennas and have the capability to process their outputs coherently, allowing for the extraction of spatial information from the observed wavefield. This is possible if the antenna outputs are sampled at a sufficiently high rate to allow for the fine timing accuracy needed in coherent spatial processing. A multiple-antenna IR-UWB receiver designed for AOA estimation of the transmitted signal will therefore require a much higher level of sophistication than a single-antenna receiver performing basic TOA estimation. Nevertheless, considering the advantages brought about by the use of AOA information in the localization process, and motivated by promising advances in the field of IR-UWB electronics, especially analog-to-digital (A/D) converter and demodulator functionality [19], there has been much interest lately toward the investigation of new algorithms with improved performance for the joint TOA/AOA estimation of radio pulses with an antenna array.

Some initial attempts in AOA estimation for UWB signals focused on subspace-based methods [20], [21]. To apply the traditional subspace method (as in the narrowband case) to UWB signals, a focusing technique must be employed [20] to account for the dependence of the steering vector on the frequency. However, the resulting algorithms are characterized by very high complexity (due to focusing, eigenvalue decomposition, etc.) and poor estimation performance in rich multipath environments. Recently, many researchers proposed to jointly estimate the TOA and AOA at low computational cost using simplified search techniques. These joint estimation schemes normally require the use of a receiver equipped with an antenna array, such as a uniform linear array (ULA) or a uniform circular array (UCA). In [22], a beamforming approach is proposed, in which the path overlapping effect is mitigated by multipath-aided acquisition. Meanwhile, time difference of arrival (TDOA)-based methods are adopted in many other works. In [23], a joint TOA/AOA estimator is proposed for UWB indoor ranging under LOS operating conditions, in which signal samples obtained from an antenna array at the Nyquist rate are processed in a three-step algorithm to produce the desired estimates. In [24], joint estimation is achieved through calculating a two dimensional delay-angle power spectrum within the frequency domain. In [25], a frequency domain approach is also adopted for the estimation of the TOA and the AOA.

In general, the TDOA-based methods first obtain TOA estimates at each antenna (either via time- or frequency-domain processing), and then extract the desired AOA by computing TDOAs. Although their performance is competitive to early schemes [20], [21], the imposed processing structure on the AOA estimation limits the achievable accuracy and suggests that other estimators with better performance may exist.

In this paper we present a full-fledged extension and study of the concepts introduced in [26], where we proposed a novel joint estimator of TOA and AOA for a multi-antenna IR-UWB receiver based on the ML criterion. Our approach is motivated by the works in [27] and [28] where the channel model is decomposed into distinct parts corresponding to early and late arrivals. Specifically, we consider a statistical signal model of the received signals in which the primary pulse image and the superposition of the secondary images are represented by a deterministic component and a zero-mean Gaussian random process, respectively. Within this context, the main contributions of this work can be summarized as follows:

- Introduction of a gating function along with the APDP in the wideband space–time correlation function of the received secondary images in order to represent the onset and subsequent decay of the secondary paths.
- Exploitation of this model to derive a previously unknown form of the log likelihood function (LLF) for the joint ML estimation of the TOA and AOA parameters.
- Derivation of the associated Cramer–Rao bounds (CRBs). In the derivation, the Fisher information matrix (FIM) with respect to both the desired parameters (TOA and AOA) and nuisance parameters (primary pulse image and APDP) is considered.
- Development of a complete method in 2-steps for the application of the proposed joint ML estimator under practical conditions of operation, including LS fitting of the APDP in the first step based on [16], [17] which is not found in prior methods.
- Discussion of the implementation aspects and investigation of the numerical complexity of the proposed method.
- Demonstration of the advantages of the proposed methods through exhaustive numerical simulations with realistic UWB channel models featuring both diffuse and directional secondary image fields.

We note that in both simulation scenarios, our proposed estimation approach exhibits superior performance to that of a competing method from the recent literature.

The rest of this paper is organized as follows. In Section II, we present the IR-UWB system model under study and formulate the estimation problem in mathematical terms. In Section III, we derive a general LLF expression for this problem and expose the processing structure of the joint ML estimator of the TOA and AOA. In Section IV, CRBs for both TOA and AOA are derived for the proposed multipath signal model. In Section V, we discuss practical aspects related to the implementation of the new estimator, especially the coarse estimation of the TOA and APDP in the first step, and the implementation of the two-dimensional search in the second step. Section VI presents the methodology and results of the numerical simulation for the two special cases mentioned above, including comparisons to the CRB. Finally, Section VII concludes the work.

II. System Model and Problem Formulation

We consider a UWB localization system as depicted in Fig. 1, in which a UWB emitter equipped with a single antenna transmits an IR-UWB signal. The transmitted signal propagates through a multi-path environment where it is reflected, scattered or diffracted by walls and other objects or surfaces. A receiver equipped with an antenna array acquires the propagating UWB signal and estimates relevant parameters (i.e., TOA and AOA), which will be used later for the source localization.

As per the IEEE 802.15.4a standard, the parameter estimation is performed during the ranging preamble of a

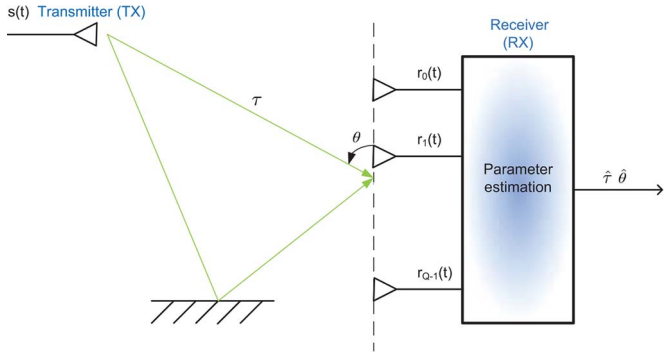

Fig. 1. UWB-based localization system.

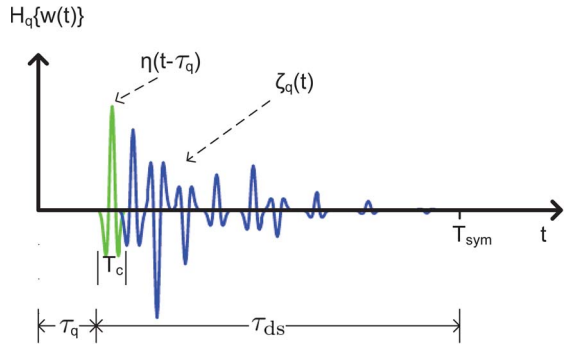

Fig. 2. Decomposition of the multi-path channel response to transmitted pulse $w(t)$ into a sum of primary, $\eta(t-\tau_q)$, and secondary, $\zeta_q(t)$, components.

synchronization header [29]. The tag-emitted signal $s(t)$ consists of $N_{\rm sym}$ consecutive pulses and is given by

$$s(t) = \sum_{j=0}^{N_{\rm sym}-1} a_j \sqrt{E_p}\, w(t - jT_{\rm sym}), \quad 0 \le t \le T_o \tag{1}$$

where $w(t)$ represents the transmitted pulse waveform, assumed to have finite duration $[0, T_c]$ and unit energy, and E_p denotes the transmitted energy per pulse. The pulse repetition period is denoted by $T_{\rm sym}$ and the transmitted signal spans a total observation time of $T_o = N_{\rm sym} T_{\rm sym}$. For the purpose of ranging, a known training sequence is adopted here, i.e., $a_j = 1,\ \forall\, j$.

The transmitted IR-UWB signal $s(t)$ propagates along multiple paths that combine additively at the receiver, where a uniform linear array (ULA) of $Q > 1$ identical antenna elements is employed for signal acquisition.[1] Under the far field assumption, the wavefronts arriving at the receiver's ULA along different paths can be taken as planar. In particular, for the primary path (the first one in a LOS environment), the TOA at the qth antenna can be written as

$$\tau_q = \tau + \left(q - \frac{Q-1}{2}\right)\Delta\tau, \quad q \in \{0, \ldots, Q-1\} \tag{2}$$

where τ denotes the TOA or propagating delay at the antenna array geometric center and $\Delta\tau$ is the TDOA between adjacent antennas. For a 2-dimensional geometry, the TDOA can be expressed in terms of the AOA, θ, as

$$\Delta\tau = \frac{d}{c}\cos\theta \tag{3}$$

where d is the inter-antenna spacing and c is the speed of light.

The propagation channel between the transmitter and the receiver's antenna array is modeled as a linear time-invariant single-input multiple-output (SIMO) system with components $\mathcal{H}_q\{\cdot\}$ where $q \in \{0, \ldots, Q-1\}$. In this work, we represent the channel response to the pulse waveform $w(t)$ at the qth antenna as a superposition of two distinct components:

$$\mathcal{H}_q\{w(t)\} = \eta(t - \tau_q) + \zeta_q(t) \tag{4}$$

[1]The use of a ULA is assumed mainly for mathematical convenience; generalization of the proposed technique to other antenna configurations is conceptually straightforward.

where $\eta(t)$ represents the pulse image arriving along the primary path and $\zeta_q(t)$ represents the total contribution (linear superposition) of the images received along secondary paths, i.e., excluding the primary one. This signal structure is depicted in Fig. 2, where the duration of $\eta(t)$ is shown comparable to that of $w(t)$, while that of the secondary images extends from around τ_q to $\tau_q + \tau_{\rm ds}$, where $\tau_{\rm ds}$ is the delay spread of the channel. Note that there may be overlap between the primary and secondary pulse images. In addition, we assume there is no interference between successive pulses, i.e., $\tau_{\rm ds} < T_{\rm sym}$. In IR-UWB localization, $s(t)$ has a low duty cycle of the order of 1 Mbit/s or less, while $\tau_{\rm ds}$ for a typical indoor channel is on the order of a few 100 ns or less. This assumption is therefore well justified from a practical standpoint and it is common in the literature (e.g., [7]).

We model the primary pulse image $\eta(t)$ as a deterministic signal, which may possibly include some unknown (nuisance) parameters. A simple such description is $\eta(t) = aw(t)$, where a denotes a (real) path gain. However, more sophisticated filtering operations can be applied to model pulse distortion resulting from the fine (time-unresolvable) structure of the channel or the receiver front-end filters. In this setting, the filtering parameters will be deterministic but unknown, and can be estimated jointly with the desired TOA and AOA.

The superimposed secondary pulse images $\zeta_q(t)$ are modeled as independent Gaussian random processes with zero mean. The Gaussian assumption can be justified in part on the basis of the central limit theorem since at any given time, the value of $\zeta_q(t)$ results from the additive contribution of a large number or nearly independent random channel taps. If in addition these taps obey a Gaussian distribution, then of course the Gaussian assumption follows immediately. In the IR-UWB literature, many works advocate the use of the Gaussian distribution for the channel taps, as in, e.g., [30] and [31], although this might come at the expense of a minor performance loss in some applications. In this work, motivated by these considerations, we propose to treat the secondary images as a Gaussian random process. We emphasize that while this choice is made in part for the sake of simplifying later derivations, nothing prevents us from utilizing the resulting estimator under conditions of operations that slightly deviate from the assumed ones.

Considering the dense indoor environments, we represent the space–time cross correlation of $\zeta_q(t)$ by

$$E\left[\zeta_q(t)\zeta_{q'}(u)\right] = \sigma_q(t)\sigma_{q'}(u)\delta_c(t-u)\varrho(q,q') \tag{5}$$

where $\delta_c(t)$ is the Dirac delta function, $\varrho(q,q')$ is the spatial correlation and $\sigma_q^2(t)$ is the instantaneous power (level) of $\zeta_q(t)$. The use of $\delta_c(t-u)$ in (5) is motivated by the fact that the extent of the temporal correlation for multipath components is usually very small [31], [32]. Regarding $\varrho(q,q')$, published results of measurement campaigns for UWB signals indicate that the spatial correlation decreases rapidly with the inter-antenna spacing [33], e.g., correlation coefficients below 0.5 for an antenna spacing of 8 cm or less [34], while the level of correlation is seen to decay substantially with spacing in excess of 10 cm [35]. In this work, considering a nominal antenna spacing of 50 cm for simplicity, we therefore set $\varrho(q,q')=1$ for $q=q'$ and 0 otherwise. Clearly, the proposed ML estimation framework in this paper could in principle be extended to more general forms of spatial correlation $\varrho(q,q')$. Nevertheless, as will be shown in Section VI, the joint estimator of the TOA and AOA developed here under this assumption can still provide very competitive results in the presence of spatial correlation.

The instantaneous power level can be further represented by

$$\sigma_q^2(t) = g(t-\tau_q)P(t) \tag{6}$$

where $P(t)$ is the APDP and $g(t)$ is a gating function. Specifically, the APDP models the decay in the small-scale average power of the received pulse images as a function of the propagating delay, for an impulse emitted at time $t=0$. The above assumption is motivated by [36], where intensive channel measurements were done in different environments with a finely spaced measurement grid and consequently, a tapped-delay-line channel model was proposed whose APDP is modeled by a single exponential with a random decay constant. In this work, it is assumed that $P(t)$ is a slowly-varying function of time relative to the pulse duration and travel time across the antenna array. Therefore, the gating function $g(t)$ is introduced to model the onset of the secondary pulse images after the primary one at $t=\tau_q$ and is assumed to satisfy the following conditions: $g(t)=0$ for $t\le 0$, $g(t)=1$ for $t\ge T_c$ and $g(t)$ is increasing for $0<t<T_c$.

Finally, the noisy IR-UWB signal received at the qth antenna at time t can be expressed as

$$\begin{aligned} r_q(t) &= \mathcal{H}_q\left\{s(t)\right\} + n_q(t) \\ &= \mu_q(t) + \xi_q(t) + n_q(t), \quad 0 \le t \le T_o \end{aligned} \tag{7}$$

where, after making use of (1) and (4), we find

$$\mu_q(t) = \sum_{j=0}^{N_{\rm sym}-1} \sqrt{E_p}\,\eta(t-\tau_q-jT_{\rm sym}) \tag{8}$$

$$\xi_q(t) = \sum_{j=0}^{N_{\rm sym}-1} \sqrt{E_p}\,\zeta_q(t-jT_{\rm sym}) \tag{9}$$

and $n_q(t)$ is an additive noise term modeled as a spatially and temporally white Gaussian process with zero mean and known power spectral density level σ_n^2. We assume that the noise terms $n_q(t)$ are statistically independent from the secondary pulse images $\zeta_{q'}(t)$.

The problem addressed in this paper can be stated as follows. Given the received antenna signals $\{r_q(t)\}$ for $0\le t\le T_o$ with $q\in\{0,\ldots,Q-1\}$, we seek to jointly estimate the TOA τ and AOA θ of the primary path. The estimated τ and θ are needed for localizing the transmitter (see (2) and (3)). A key feature of our proposed approach is the formal consideration of distinct models for the primary pulse image $\eta(t)$ and the combined secondary images $\zeta_q(t)$, and especially the use of the space–time correlation function (5) and (6) which incorporates the gating and APDP functions. This formulation will allow us to derive a new ML estimator with improved performance and gain a deeper insight into its operation. While we shall consider the effect of unknown (nuisance) parameters of $\eta(t)$ and $\zeta_q(t)$ on the estimation process, our main interest lies in the estimation of the geometrical TOA and AOA parameters. Appropriately, in our proposed approach, it will be sufficient to use educated guesses of the functions $\eta(t)$, $g(t)$ and $P(t)$ in order to benefit from the merits of the ML formulation. The choice of these functions will be further discussed in Sections V and VI.

III. Joint Maximum Likelihood Estimation

In this section, we first derive the LLF for the SIMO system model previously introduced. We then formulate the joint ML estimator of the TOA and AOA parameters which will play a key role in our proposed scheme.

In practice, the received antenna signals $r_q(t)$ are uniformly sampled at a rate F_s which is greater than or equal to the Nyquist rate. Therefore, we let $t=nT_s$, where n is an integer and $T_s=1/F_s$ denotes the sampling period which meets the Nyquist criterion for bandpass signals. In addition, for the sake of simplicity, we assume that each pulse repetition period consists of exactly M time samples, i.e., $T_{\rm sym}=MT_s$ where M is a positive integer.

Let us represent the set of received antenna signals during the jth symbol by the vector function

$$\mathbf{r}_j(t) = \left[r_0(t+jT_{\rm sym}),\ldots,r_{Q-1}(t+jT_{\rm sym})\right]^T \tag{10}$$

where $r_q(t+jT_{\rm sym})$ is given by (7) and discrete-time $t\in\mathcal{T}=\{nT_s : n=0,1,\ldots,M-1\}\subset[0,T_{\rm sym})$. In the absence of interference between adjacent pulses, with t restricted in this manner, it follows from (8) and (9) that $\mu_q(t+jT_{\rm sym}) = \sqrt{E_p}\eta(t-\tau_q)$ and $\xi_q(t+jT_{\rm sym})=\sqrt{E_p}\zeta_q(t)$, respectively. Therefore, we can write

$$\mathbf{r}_j(t) = \boldsymbol{\mu}(t) + \boldsymbol{\xi}(t) + \mathbf{n}_j(t) \tag{11}$$

where we define

$$\boldsymbol{\mu}(t) = \sqrt{E_p}\left[\eta(t-\tau_0),\ldots,\eta(t-\tau_{Q-1})\right]^T \tag{12}$$

$$\boldsymbol{\xi}(t) = \sqrt{E_p}\left[\zeta_0(t),\ldots,\zeta_{Q-1}(t)\right]^T \tag{13}$$

$$\mathbf{n}_j(t) = \left[n_0(t+jT_{\rm sym}),\ldots,n_{Q-1}(t+jT_{\rm sym})\right]^T. \tag{14}$$

We note that due to the repetitive nature of the transmitted pulse sequence (and the fact that $a_j = 1$) in (1), the primary and secondary image components received over consecutive pulse periods are identical, i.e., $\boldsymbol{\mu}(t)$ and $\boldsymbol{\xi}(t)$ in (11) do not depend on the symbol index j.

In the context of IR-UWB localization, the received pulse train is usually averaged to increase the SNR. Letting $\mathbf{x}(t) = [x_0(t), \ldots, x_{Q-1}(t)]^T$ denote the symbol-averaged array output vector, it follows from (11) that

$$\mathbf{x}(t) = \frac{1}{N_{\text{sym}}} \sum_{j=0}^{N_{\text{sym}}-1} \mathbf{r}_j(t) = \boldsymbol{\mu}(t) + \boldsymbol{\xi}(t) + \mathbf{n}(t) \tag{15}$$

where the additive noise term $\mathbf{n}(t) = (1/N_{\text{sym}}) \sum_j \mathbf{n}_j(t)$.

Invoking the Gaussian assumption on the secondary images and background noise processes, it follows that $\mathbf{x}(t)$ is a Gaussian vector process with non-zero mean, $E[\mathbf{x}(t)] = \boldsymbol{\mu}(t)$, and $Q \times Q$ matrix auto-covariance function

$$\begin{aligned}\mathbf{K}_x(t,u) &= E\left[(\mathbf{x}(t) - \boldsymbol{\mu}(t))(\mathbf{x}(u) - \boldsymbol{\mu}(u))^T\right] \\ &= \mathbf{K}_\xi(t,u) + \mathbf{K}_n(t,u)\end{aligned} \tag{16}$$

where, in turn, $\mathbf{K}_\xi(t,u) = E[\boldsymbol{\xi}(t)\boldsymbol{\xi}(u)^T]$ and $\mathbf{K}_n(t,u) = E[\mathbf{n}(t)\mathbf{n}(u)^T]$ denote the auto-covariance functions of $\boldsymbol{\xi}(t)$ and $\mathbf{n}(t)$, respectively. In these expressions, u is a discrete-time variable with the same range as t. Using the expressions (5) and (6) of the space–time cross-correlation function of $\zeta_q(t)$, and taking into account the band-limited (i.e., anti-aliasing) filtering implicit in the uniform sampling of the antenna signals, we obtain

$$\mathbf{K}_\xi(t,u) = E_p \delta(t-u) \mathbf{D}(t) \frac{1}{T_s} \tag{17}$$

where $\delta(t)$ is the Kronecker delta function[2] and $\mathbf{D}(t)$ is a $Q \times Q$ diagonal matrix with qth diagonal entry $\sigma_q^2(t)$. Meanwhile, we have

$$\mathbf{K}_n(t,u) = \sigma_{\bar{n}}^2 \delta(t-u) \mathbf{I}_Q \frac{1}{T_s} \tag{18}$$

where we define $\sigma_{\bar{n}}^2 = \sigma_n^2 / N_{\text{sym}}$ and $\mathbf{I}_Q$ is the identity matrix of order Q.

Let the unknown parameters under estimation be represented by the row vector $\boldsymbol{\phi} = [\tau, \theta, \boldsymbol{\phi}_\eta, \boldsymbol{\phi}_\zeta]$, where $\boldsymbol{\phi}_\eta$ contains the (nuisance) parameters associated to the pulse image from the primary path, $\eta(t)$, and $\boldsymbol{\phi}_\zeta$ contains those associated to the pulse images from the secondary paths, $\{\zeta_q(t)\}_{q=0}^{Q-1}$. Also let $\boldsymbol{x}$ denote the complete set of symbol-averaged array output vectors available for estimation, i.e., $\{\mathbf{x}(t) : t \in \mathcal{T}\}$. For the non-zero mean Gaussian signal model under consideration in this study, the LLF of the observations can be expressed (up to a constant factor) in the form [37]

$$\ln \Lambda(\mathbf{x}; \boldsymbol{\phi}) = -\frac{1}{2} \left(l_1(\mathbf{x}; \boldsymbol{\phi}) + l_2(\boldsymbol{\phi}) \right) \tag{19}$$

[2]That is, $\delta(nT_s)$ is equal to 1 for $n = 0$ and to 0 for all integers $n \neq 0$.

where the two terms composing this expression are examined in detail below.

The data-dependent term $l_1(\mathbf{x}; \boldsymbol{\phi})$ is given by

$$l_1(\mathbf{x}; \boldsymbol{\phi}) = \sum_{t \in \mathcal{T}} \sum_{u \in \mathcal{T}} (\mathbf{x}(t) - \boldsymbol{\mu}(t))^T \mathbf{K}_x^{-1}(t,u) (\mathbf{x}(u) - \boldsymbol{\mu}(u)) \tag{20}$$

where the quantity $\mathbf{K}_x^{-1}(t,u)$ denotes the inverse kernel of the auto-covariance function $\mathbf{K}_x(t,u)$ in (16), and is obtained as the solution to the inverse problem:

$$\sum_{u \in \mathcal{T}} \mathbf{K}_x(t,u) \mathbf{K}_x^{-1}(u,v) = \delta(t-v), \quad (t,v) \in \mathcal{T}^2. \tag{21}$$

For the special form of the auto-covariance function in (16), it can be verified that the solution to (21) is given by:

$$\mathbf{K}_x^{-1}(t,u) = \delta(t-u) T_s \left(E_p \mathbf{D}(t) + \sigma_{\bar{n}}^2 \mathbf{I}_Q \right)^{-1}. \tag{22}$$

Substituting this expression in (20), and after further manipulations, we find that

$$l_1(\mathbf{x}; \boldsymbol{\phi}) = T_s \sum_{q=0}^{Q-1} \sum_{t \in \mathcal{T}} \frac{\left[x_q(t) - \sqrt{E_p} \eta(t - \tau_q) \right]^2}{E_p g(t - \tau_q) P(t) + \sigma_{\bar{n}}^2}. \tag{23}$$

The second term, $l_2(\boldsymbol{\phi})$ in (19), is given by

$$l_2(\boldsymbol{\phi}) = \ln \det \mathcal{K} \tag{24}$$

where $\mathcal{K}$ is a Hermitian matrix of order MQ, composed of M^2 blocks of size $Q \times Q$, with $\mathbf{K}_x(t,u)$ as its (t,u)th block. In the situation of interest here, due to the presence of the delta function in $\mathbf{K}_x(t,u)$ (16)–(18), $\mathcal{K}$ is block diagonal and so this term simplifies naturally to

$$\begin{aligned} l_2(\boldsymbol{\phi}) &= \sum_{t \in \mathcal{T}} \ln \det \mathbf{K}_x(t,t) \\ &= T_s \sum_{q=0}^{Q-1} \sum_{t \in \mathcal{T}} \ln \left[E_p g(t - \tau_q) P(t) + \sigma_{\bar{n}}^2 \right]. \end{aligned} \tag{25}$$

The LLF terms $l_1(\mathbf{x}; \boldsymbol{\phi})$ (23) and $l_2(\boldsymbol{\phi})$ (25) depend on the unknown TOA/AOA parameters τ and θ through the intermediate TOA variable τ_q, as per (2) and (3), while their dependence on the nuisance parameters ϕ_η and ϕ_ζ is through the functions $\eta(t)$ and $P(t)$, respectively.

Given the set $\mathbf{x}$ of symbol-averaged array output vectors, the ML estimator of the parameter vector $\boldsymbol{\phi}$ is obtained by maximizing the LLF $\ln \Lambda(\mathbf{x}; \boldsymbol{\phi})$ (19), or equivalently:

$$\hat{\boldsymbol{\phi}}_{\text{ML}} = \arg \min_{\boldsymbol{\phi} \in \mathcal{P}} \left(l_1(\mathbf{x}; \boldsymbol{\phi}) + l_2(\boldsymbol{\phi}) \right) \tag{26}$$

where $l_1(\mathbf{x}; \boldsymbol{\phi})$ and $l_2(\boldsymbol{\phi})$ are given by (23) and (25), respectively, and $\mathcal{P}$ denotes the parameter space over which the search is performed. In practice, the search range for the TOA and AOA parameters, i.e., τ and θ, respectively, will be restricted by geometrical considerations. This aspect is further discussed in Section V. Other limitations may apply to the search ranges of the nuisance parameters in $\boldsymbol{\phi}_\eta$ and $\boldsymbol{\phi}_\zeta$ when they are part of the estimation process.

It is worth noting that, for $l_2(\boldsymbol{\phi})$, the inner sum over t is almost the same for the different possible values of the unknown delay τ and differential delay $\Delta\tau$. Indeed, as long as the

channel delay spread is smaller than the pulse repetition period $T_{\rm sym}$, the value of this term is almost constant. Therefore, maximizing the data dependent term $l_1(\mathbf{x};\boldsymbol{\phi})$ with respect to τ and θ is our main consideration. This term dictates the signal processing operations that need to be performed on the observed data $\mathbf{x}$ to obtain $\hat{\boldsymbol{\phi}}_{\rm ML}$. Upon closer examination of (23), we note that the ML processing is tantamount to obtaining, for each antenna index q, the best match between $x_q(t)$ and $\sqrt{E_p}\eta(t-\tau_q)$ during the initial period, while ensuring that the instantaneous power in the residual signals $x_q(t)-\sqrt{E_p}\eta(t-\tau_q)$ conforms to the available *a priori* information about the APDP. In the low SNR regime where $E_p \ll \sigma_{\bar{n}}^2$, the ML processor simply measures and seeks to minimize the energy of the difference signals at the Q antennas over the symbol duration.

IV. CRB Analysis

Although closed form expressions for the CRB of TOA and AOA estimation can be found in previous works [22], [38], the CRB for the signal model considered here still needs to be investigated.

As discussed in the previous section, of the four elements comprising the unknown parameter vector $\boldsymbol{\phi}=[\tau,\theta,\boldsymbol{\phi}_\eta,\boldsymbol{\phi}_\zeta]=[\phi_1,\phi_2,\phi_3,\phi_4]$ we are interested in just the first two, τ and θ. The first step towards the derivation of the CRB of τ and θ is to evaluate the FIM $\boldsymbol{J}$ with elements $J_{i,j}$ given by

$$J_{i,j}=-E\left[\frac{\partial^2 \ln \Lambda(\mathbf{x};\boldsymbol{\phi})}{\partial\boldsymbol{\phi}_i\partial\boldsymbol{\phi}_j}\right],\ i,j\in\{1,2,3,4\}. \tag{27}$$

Closed form expressions for the entries of the FIM are derived in Appendix A. We should note that in Appendix A, we consider the general forms of the nuisance parameters $\boldsymbol{\phi}_\eta$ and $\boldsymbol{\phi}_\zeta$; in practice, each of them may consist of more than one parameters, depending on the exact form adopted.

Since we are only interested in the first two unknown parameters, τ and θ, we partition $\boldsymbol{J}$ as follows

$$\mathbf{J}=\begin{bmatrix}\mathbf{A} & \mathbf{C}\\ \mathbf{C}^T & \mathbf{B}\end{bmatrix} \tag{28}$$

where $\boldsymbol{A}$ is the 2×2 FIM corresponding to τ and θ, $\boldsymbol{B}$ is the FIM corresponding to the nuisance parameters $\boldsymbol{\phi}_\eta$ and $\boldsymbol{\phi}_\zeta$, and finally $\boldsymbol{C}$ depends on all the unknown parameters. Accordingly, we calculate the equivalent FIM (EFIM) [18], [22] whose inverse $\left(\boldsymbol{A}-\boldsymbol{C}\boldsymbol{B}^{-1}\boldsymbol{C}^T\right)^{-1}$ will provide the CRB of τ and θ. After some further calculations we have

$$\text{CRB}(\tau)=\left(J_{11}-J_{13}J_{33}^{-1}J_{31}-J_{14}J_{44}^{-1}J_{41}\right)^{-1} \tag{29}$$

$$=\frac{1}{Q\left(S-S^{13}r_3-S^{14}r_4\right)} \tag{30}$$

where S, S^{13}, and S^{14} are constants defined in Appendix A,

$$r_3=\sum_{t\in\mathcal{T}}\frac{\eta'(t-\tau_q)}{\gamma(t,\tau_q)}\frac{\partial\eta(t-\tau_q)}{\partial\boldsymbol{\phi}_\eta}\Bigg/\sum_{t\in\mathcal{T}}\frac{1}{\gamma(t,\tau_q)}\left(\frac{\partial\eta(t-\tau_q)}{\partial\boldsymbol{\phi}_\eta}\right)^2 \tag{31}$$

and

$$r_4=\sum_{t\in\mathcal{T}}\frac{1}{\gamma^2(t,\tau_q)}\frac{\partial\gamma(t,\tau_q)}{\partial\boldsymbol{\phi}_\zeta}\frac{\partial\gamma(t,\tau_q)}{\partial\tau}\Bigg/\sum_{t\in\mathcal{T}}\frac{1}{\gamma^2(t,\tau_q)}\left(\frac{\partial\gamma(t,\tau_q)}{\partial\boldsymbol{\phi}_\zeta}\right)^2. \tag{32}$$

Also,

$$\text{CRB}(\theta)=J_{22}^{-1}=\frac{c^2}{Sd^2(\sin\theta)^2\Psi}. \tag{33}$$

Regarding S we note that it can be written as

$$S=\text{SNR}(S_A+S_B) \tag{34}$$

with

$$S_A=T_s\sum_{t\in\mathcal{T}}\frac{\eta'(t-\tau)^2}{1+\text{SNR}g(t-\tau)P(t)} \tag{35}$$

$$S_B=\frac{T_s}{2}\sum_{t\in\mathcal{T}}\frac{\text{SNR}g'(t-\tau)^2P(t)^2}{\left(1+\text{SNR}g(t-\tau)P(t)\right)^2} \tag{36}$$

where the SNR is defined as $\text{SNR}=E_p/\sigma_{\bar{n}}^2$.

We can now make the following observations:

- In the absence of secondary paths, $g(t)=0$ and S reduces to

$$S=T_s\text{SNR}\sum_{t=0}^{T_c/T_s}\eta'(t)^2. \tag{37}$$

  In this case, (29) and (33) are identical to the conventional form of the CRB found in the literature [22], [38].
- In practice, the transmitted signal will be subjected to multipath, i.e., $g(t)\neq 0$. If there is overlap between the primary and secondary images (in which case, the overlapping secondary images act as interference in the estimation), the denominator in (35) will be larger than $\sigma_{\bar{n}}^2$ over a corresponding time interval. Therefore, the value of S_A will be reduced and, in turn, this will contribute to increase the CRB. A related discussion can be found in [22].
- Recall that $g(t)$ is used to characterize the onset of the secondary paths. Therefore, the instantaneous power level of the secondary images, as given by $\sigma_q^2(t)$ in (6), provides some information about the unknown delay τ_q through the function $g(t-\tau_q)$. In this respect, a fast transition in the term $g(t)$, as in the limiting case of $g(t)=u(t-T_c)$, would contribute to an increase in the term S_B in (36), and thereby reduce the CRB.
- Finally, we note that the achievable performance of both TOA and AOA estimators depends on the pulse shape, SNR, total number of antennas Q, and the number of symbols $N_{\rm sym}$ in the observation period. While the analysis was carried out for a ULA, the use of a different array geometry would also affect the performance.

These properties of CRB shed additional light on the achievable performance level of joint TOA/AOA estimators in the presence of overlapping primary and secondary images.

V. Practical Realization of the Joint ML Estimator

According to the developments in Section III, in order to obtain the joint ML estimates of the unknown TOA and AOA parameters we need to minimize the data dependent term of the LLF, as given by expression (23). Assuming that the APDP $P(t)$ and the primary pulse image $\sqrt{E_p}\eta(t)$ are known *a priori*, this minimization can be performed in theory by carrying a full two-dimensional search over the set of permissible values for τ and θ. The computational cost associated with a full search is, however, prohibitive and this approach is not feasible in practice. Here, we consider a low-cost alternative that consists of two steps: In the first step, we perform a preliminary estimation of the TOAs τ_q, based on which we then obtain suitable estimates of $P(t)$ and $\sqrt{E_p}\eta(t)$. In the second step, using the obtained estimates, we find the best combination of τ and θ that minimizes (23) via a simplified search strategy that takes advantage of the preliminary TOAs along with localized time domain interpolation. The detailed description below covers the following aspects: preliminary TOA estimation, subsequent estimation of *priori* information (i.e., APDP and primary pulse image), two dimensional search of LLF for optimum parameters with interpolation, and finally, complexity analysis.

A. Preliminary TOA Estimation

As with many other high-resolution techniques for joint TOA/AOA estimation of UWB signals, our proposed approach will require a preliminary estimation of the unknown TOAs in order to reduce the size of the search space and minimize the complexity of the final estimation. Several low-complexity TOA estimators are available for this purpose from the literature. Among these, energy detection approaches that do not require explicit knowledge of the pulse shape are well suited for this task. In particular, a simple energy detector based on a threshold crossing (TC) as in [39] can be adopted for this purpose. This technique can be applied at a single antenna or independently at multiple antennas, followed by averaging of the multiple TOA estimates.

Specifically, in the TC-based method, the TOA estimate at the qth antenna is obtained as the smallest value of time t for which the instantaneous power at the antenna output, $x_q^2(t)$, exceeds a given threshold λ. That is

$$\hat{\tau}_q = \min_{0<t<T_u} \left\{ t : x_q^2(t) > \lambda \right\} \tag{38}$$

where T_u is the initial search range (uncertainty region) for the TOA. In our work, the value of the threshold λ is obtained by first finding the value of λ which minimizes the theoretical MSE of the TOA estimator based on energy detection as in [39], and then experimentally fine-tuning λ to improve the TOA estimation performance considering the trade-off between the probabilities of false alarm and missed detection. We have been able to verify that the final estimation performance of the proposed joint TOA/AOA estimator is not overly sensitive to the particular choice of the threshold being used for TC in the preliminary TOA estimation step. Once TOA estimates $\hat{\tau}_q$ are obtained for each one of the antennas, we can further compute an LS estimate of τ as [23], [25]

$$\hat{\tau}_{LS} = \frac{1}{Q} \sum_{q=0}^{Q-1} \hat{\tau}_q. \tag{39}$$

B. Estimation of a priori Information

The required *a priori* information needed to implement the proposed joint ML estimator consists of two main elements, namely: the APDP $P(t)$ and the primary pulse image $\sqrt{E_p}\eta(t)$. In practice, this information may not be readily available and it therefore needs to be estimated beforehand. In this work, the required *a priori* information is obtained separately through simplified estimators to limit the processing complexity. Still, as will be shown in Section VI, this is adequate to obtain significant performance gains in the ML-based joint TOA/AOA estimation. Below, we discuss in further details the determination of $P(t)$ and $\sqrt{E_p}\eta(t)$.

In the context of UWB propagation, the APDP is typically modeled as the superposition of doubly-exponential decaying clusters with Poisson inter-arrival times, as per the Saleh-Valenzuela model [40]. Here, we propose the use of a single decaying exponential, as given by[3]

$$P(t) = \beta e^{-\alpha t} \tag{40}$$

where $\alpha > 0$ is the decay rate and β is the peak power level. To estimate the APDP, we propose to fit the instantaneous power at the output of a selected antenna to this model. Let $l_o = \lfloor \hat{\tau}_{LS}/T_s \rfloor$ and $L = \lfloor \tau_{ds}/T_s \rfloor$ respectively denote the LS estimate of τ and the maximum channel delay spread in samples, with $\lfloor \cdot \rfloor$ being the floor function. More specifically, we seek the choice of α and β that provides the best fit between the segment $P_0(l) = x_0((l_o + l)T_s)^2$ for $l \in \{0, \ldots, L-1\}$, and the function $\beta e^{-l\alpha}$. We perform the curve fitting in the log domain using a weighted LS criterion, i.e.,

$$(\hat{\alpha}, \hat{\beta}) = \arg\min_{\alpha,\beta} \sum_{l=0}^{L-1} \mu_l \left| \ln P_0(l) - (\ln \beta - l\alpha) \right|^2. \tag{41}$$

In this approach, we set $\mu_l = 1$ if there is a local maximum, i.e., $P_0(l-1) < P_0(l)$ and $P_0(l) > P_0(l+1)$, and $\mu_l = 0$ otherwise. This choice of μ_l allows us to include in the fitting only the local maxima, as they are more likely to correspond to multipath components, and to mask out the noisy low power data points [16], [17]. Denoting as $\hat{\beta}$ and $\hat{\alpha}$ the solutions to (41), we obtain a preliminary estimate of the APDP as

$$\hat{P}(nT_s) = \hat{\beta} e^{-\hat{\alpha}(n - l_o)}, \quad n = 0, \ldots, M-1. \tag{42}$$

We note that the initial samples of $\hat{P}(t)$ are not critical in (23) since they will be zeroed by the gating function $g(t - \tau_q)$.

[3]While in principle, it is possible to use a multi-cluster model for the APDP, i.e., superposition of multiple decaying exponentials, we have found through simulations that the use of the single exponential model (40) is adequate to exploit the main benefits of the weighting mechanism inherent in the LLF (23). Considering its simplicity, this model is therefore adopted in this work.

Due to local (small-scale) channel dispersion as well as the effects of the transmit and receive filters, the shape of the primary pulse image $\eta(t)$ will be distorted when compared to the originally transmitted pulse waveform $w(t)$. This distortion can be significant and, in general, we find that, for the type of multipath channels under consideration in this work, the use of the known pulse shape $w(t)$ in place of $\eta(t)$ does not give satisfactory results in the joint TOA/AOA estimation. Therefore, it is necessary to estimate the scaled primary image $\sqrt{E_p}\eta(t)$ prior to carrying out the search for the minimizers of (23). In our proposed approach, an estimate of this quantity is obtained simply as a time-shifted version of $x_0(t)$ over an interval of duration T_c. Specifically, for each candidate value of τ, we replace the function $\sqrt{E_p}\eta(t)$ in (23) by

$$\sqrt{E_p}\hat{\eta}(t;\tau) = x_0(t+\tau), \quad 0 \le t < T_c. \tag{43}$$

As will be demonstrated through simulations, this approach is robust to small-scale distortion and leads to satisfactory performance in the absence of exact knowledge of the received pulse shape.

C. Parameter Search and Interpolation

With the assumed knowledge of the APDP $P(t)$ and primary pulse image $\sqrt{E_p}\eta(t)$, the joint ML estimator of the TOA τ and AOA θ can now be obtained as the minimizers

$$(\hat{\tau}, \hat{\theta}) = \arg \min_{(\tau,\theta)\in\mathcal{P}} l_1(\mathbf{x};\tau,\theta) \tag{44}$$

where the objective function is computed according to (23) and $\mathcal{P}$ is the set of permissible values over which the two-dimensional search is performed. The choice of the search space $\mathcal{P}$ is further discussed in Part D below.

Once a local optimizer has been found, refined estimates of the desired parameters with improved resolution can be obtained through a final interpolation of the objective function. That is, the time dependent terms in (23) will be replaced by their interpolated versions and the two-dimensional search will be resumed with a finer step size near the previously found minimizer. In the sequel, we refer to the refined search step as $T_{\rm int}$, which is typically set to $T_s/K_{\rm int}$, where $K_{\rm int}$ is a positive integer. In this work, we use interpolation based on quadratic polynomial fit, but other interpolation methods could be used as well. The performance of the proposed estimator depends on the final value of $T_{\rm int}$, and in general, a reduction of the value of this parameter contributes to a decrease in the estimator variance. However, the trade-off between accuracy and complexity should always be considered.

D. Numerical Complexity

In addition to its superior performance (see Section VI), one advantage of the proposed joint estimator of the TOA and AOA is the relatively moderate computational complexity of its realization, as explained below.

In the first step, the main computation cost lies in the preliminary estimation of the TOA and the APDP. According to the TC method, once a suitable threshold λ has been chosen in (38), the TOA estimation cost is mainly dictated by the size of the search range, and is therefore upper bounded by $Q\lfloor T_u/T_s \rfloor$. The LS estimation of the APDP aims to represent a set of power measurements by a straight line in the log domain, or equivalently, a product $\boldsymbol{Av}$, where $\boldsymbol{A}$ is a known matrix of size $m \times 2$ ($m < L$ is the number of points used) and $\boldsymbol{v} = [\alpha, \ln\beta]^T$ is the vector of unknown parameters. The efficient implementation of the LS method then involves the QR factorization of matrix $\boldsymbol{A}$, with a cost of $8m$, followed by the computation of the unknown parameters with a cost of $4m$. Therefore, the total cost for the LS fitting is $12m$, which is linear in m.

In the second step, the main cost lies in the computation of the objective function (23) over the two-dimensional search range of interest. According to our previous discussion and based on further experimentation, we found that only a small search range is needed to obtain adequate estimation results. In particular, the search for the TOA will be limited to K_1 samples around the previously obtained estimate $\hat{\tau}_{LS}$, where K_1 is a small integer. The search over θ will be limited to a non-uniform set of $K_2 = 2\lfloor d/cT_s \rfloor + 1$ values given by $\theta_k = \arccos(kcT_s/d)$, where the range of $|k| \le \lfloor d/cT_s \rfloor$ depends on the antenna separation and the sampling period.

Therefore, the two-dimensional search space consists of K_1K_2 points in total, where for each point, the evaluation of (23) requires $5QL$ numerical operations. We find that the complexity of the two-dimensional search is consequently bounded by $5K_1K_2QL$ operations per application of the algorithm. In our simulations, typical values of the product K_1K_2 are of the order of 1000 or less, as will be elaborated upon in the next section. In total, the complexity of our proposed approach exceeds that of competing methods presented in [23], [25], which is understandable since the latter do not perform a two-dimensional search of the optimal TOA/AOA parameters. For instance, the final step in the method [23], which aims to refine the TDOA estimate (but not the TOA) requires the sub-Nyquist interpolation of antenna signals followed by a one-dimensional search of the unknown TDOA parameter. For this search, the total cost is on the order of $O(K_1QL_g)$ where the value of L_g is comparable to L when we take into account the sub-Nyquist interpolation. However, the lower computational complexity of this method, by a factor K_2, comes at the cost of a performance degradation in the estimation accuracy, as will be seen in Section VI.

VI. Simulation Results

In this section, computer simulations are used to evaluate the performance of the proposed joint estimator of the TOA and AOA, and the corresponding results are discussed. For completeness, results are presented for two different types of secondary image fields, i.e., diffuse and directional.

A. Methodology

We use a Gaussian doublet as the transmitted pulse $w(t)$ with 10 dB-bandwidth $B = 4.2$ GHz and central frequency 2.8 GHz;

the emission power is set at 1 mW. The other system parameters of interest on the transmitter side are chosen as follows: pulse duration $T_c = 0.5$ ns, pulse repetition period $T_{\rm sym} = 200$ ns and number of transmitted pulses $N_{\rm sym} = 1000$. The receiver is equipped with a ULA of $Q \in \{2, 3, 4\}$ identical antenna elements, with inter-element spacing $d = 50$ cm, except for the results of Fig. 6 where the antenna spacing is varied. The nominal sampling rate at the receiver is $F_s = 16$ GHz, while further interpolation can be conducted later. The UWB radio channels are generated using the models in the IEEE 802.15.4a standard [40]. To properly emulate the plane wave propagation, spatial dependence should be introduced when an antenna array is employed at the receiver. Accordingly, certain modifications are needed to account for this aspect. In particular, we generate the channel response according to model CM1 (residential LOS) and then add the spatial dependence to the model according to [41], [42]. That is, the AOA of each path follows a Laplacian distribution with a cluster mean value uniformly distributed in a given range and a standard deviation of 5° for each cluster.

For each Monte Carlo run, we synthesize a SIMO channel according to the above approach and use it to generate the received antenna signals, to which we add white Gaussian noise at the desired power level. This data is used to jointly estimate the TOA and AOA by means of our newly proposed approach, realized in two steps as described in Section V. In the first step, we set the initial search range to $T_u = 80$ ns, while in the second step, considering the above choices for the UWB setup, we use $K_1 = 17$ and $K_2 = 55$ in defining the size of the two-dimensional search space (prior to interpolation). Regarding the gating function $g(t)$ needed in the evaluation of (23), in the absence of further *a priori* knowledge, we make the simplest possible choice and use a unit step function with delay T_c. We compare our approach to the recently proposed method from [23] as well as the CRB assuming perfect *a priori* knowledge of $\eta(t)$ and $P(t)$. The performance of the joint estimators of the TOA and AOA is evaluated in terms of the root mean square error (RMSE), based on a sample size of 500 runs using independent channels and additive noise realizations, and shown plotted as a function of the SNR $= E_p/\sigma_n^2$.

B. Diffuse Image Field

This situation, which is the most typical case for UWB applications, occurs in dense, highly reverberant environments, where a large number of secondary images impinge on the receiver's antenna array from a wide range of directions. In our computer implementation of the SIMO UWB channel, this configuration is achieved by selecting the mean AOA of each cluster from a uniform distribution over the range [45°, 135°].

Fig. 3 compares the AOA estimation performance of our proposed method to that in [23] for ULAs with $Q = 3$ and 4 antennas. While the AOA estimation accuracy of both methods improves with increasing the number of antennas, it can be seen that the proposed method achieves a significantly better accuracy under the same choice of parameters. Both at low and high SNR, the RMSE of the proposed method is significantly lower than that of the reference one. In particular, in the high SNR regime for $Q = 4$, a reduction of about 9 dB in RMSE

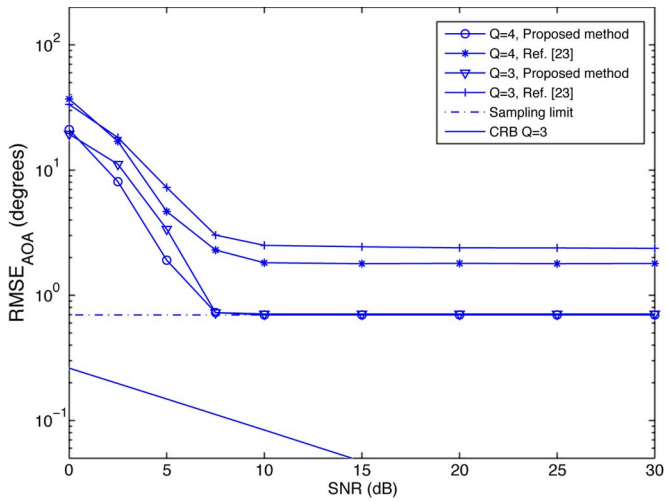

Fig. 3. RMSE of AOA estimates versus SNR for different numbers of antennas ($F_s = 16$ GHz).

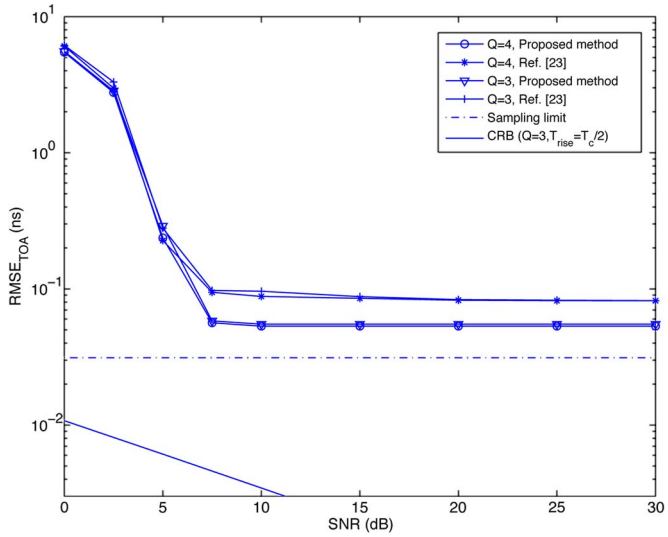

Fig. 4. RMSE of TOA estimates versus SNR for different numbers of antennas ($F_s = 16$ GHz).

is observed. Here, the attainable RMSE value of the proposed method is limited by the step size used in the ML search (represented as the sampling limit in Fig. 3). Results for TOA estimation in Fig. 4 also show a superior performance with the proposed method. In this case, as the SNR increases, there is a clear gap of about 4.5 dB between the RMSE of the two methods. Finally, regarding the quality of the APDP estimation with a single decaying exponential, we note that the value of the curve fitting error in (41), normalized by its value when $\beta = 1$ and $\alpha = 0$, averages to about 0.1 at a nominal operating SNR of 15 dB.

The relationship between accuracy in spatial localization and TOA/AOA measurement is discussed in terms of the CRB in [43]. The CRB formulas provided in this paper can be used to compute the improvement in localization accuracy that result from the smaller estimation RMSE with our proposed approach as compared to [23]. However, this requires the specification of an explicit operating configuration in terms of the number and position of the receivers, number of antennas, etc. Here,

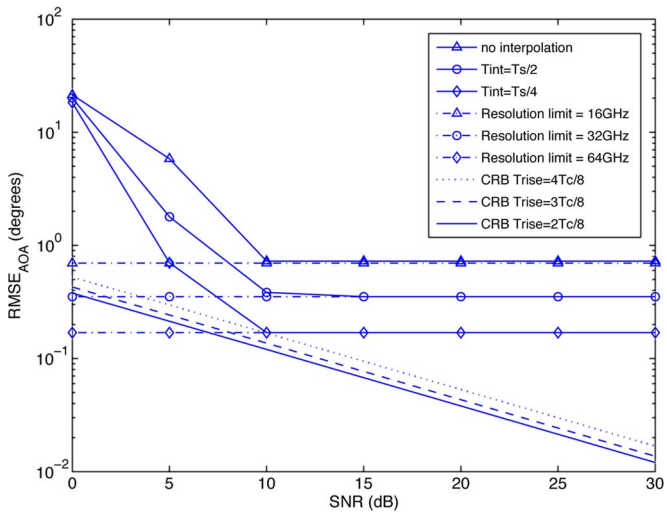

Fig. 5. RMSE of AOA estimates of proposed method versus SNR for different resolutions in the interpolation step ($Q = 2$).

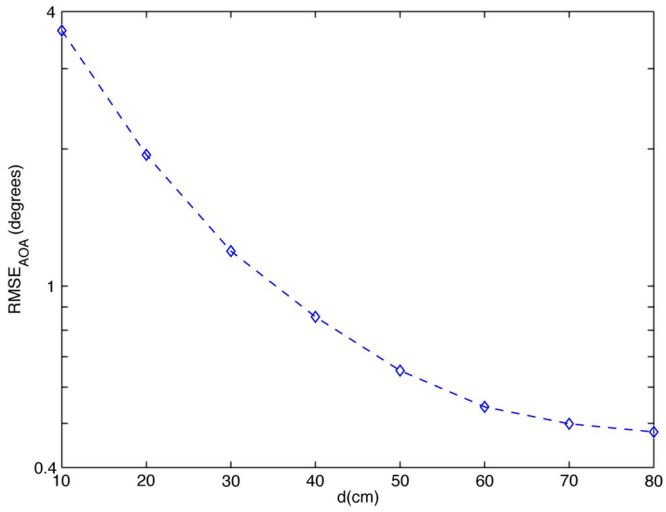

Fig. 6. RMSE of AOA estimates versus antenna spacing ($Q = 2$, SNR $=$ 20 dB).

we shall limit our discussion of this issue to a simplified scenario, that is: single receiver equipped with Q $= 3$ antennas, source node located along the array broadside ($\theta = 90^\circ$) at a distance of 4 m from array center, and SNR $= 10$ dB. For this configuration, the RMSE values in Figs. 3 and 4 translate into a radial and tangential localization RMSE of 1.5 cm and 6 cm for the proposed method, versus 3 cm and 17 cm, respectively, for [23].

Fig. 5 compares the AOA estimation performance of the proposed method with different values of the step size in the interpolation, i.e., $T_{\rm int} = T_s/2$ and $T_s/4$. It can be seen that when the resolution is finer (i.e., $T_{\rm int}$ is reduced), a better accuracy is obtained in the estimation. We note that the performance gap between the CRB and AOA estimates is reduced when the resolution is improved, although at higher SNR, the time resolution will ultimately limit the achievable performance. To study the effect of overlap between the onset of the secondary pulse images and the primary pulse period on the achievable estimation performance, we use a triangular ramp for the gating function when implementing the CRB calculations of Section IV, that is: $g(t) = 0$ for $t \le T_c - T_{\rm rise}$, $g(t) = 1$ for $t \ge T_c$ and $g(t)$ is linearly increasing for $T_c - T_{\rm rise} < t < T_c$. Here, the rise time of the ramp function, i.e., $T_{\rm rise}$, can be interpreted as the overlapping time of the secondary image pulse over the primary one.

Fig. 6 shows the AOA estimation performance of the proposed method for different values of d, i.e., the antenna spacing between two adjacent antenna elements. When d is larger, the RMSE of the AOA estimates decreases as expected. In particular, a notable gain in performance is achieved when the spacing is increased from 10 to 60 cm. Beyond this value, other effects such as the loss of spatial correlation over the primary path wavefront, would limit the estimation accuracy in practice.

In Fig. 7, we investigate the AOA estimation performance of the proposed method for different modifications of the error weighting in (23). Specifically, we seek to demonstrate the role played by the gating function $g(t - \tau_q)$ and the APDP $P(t)$ in the denominator of this expression. To this end, we compare

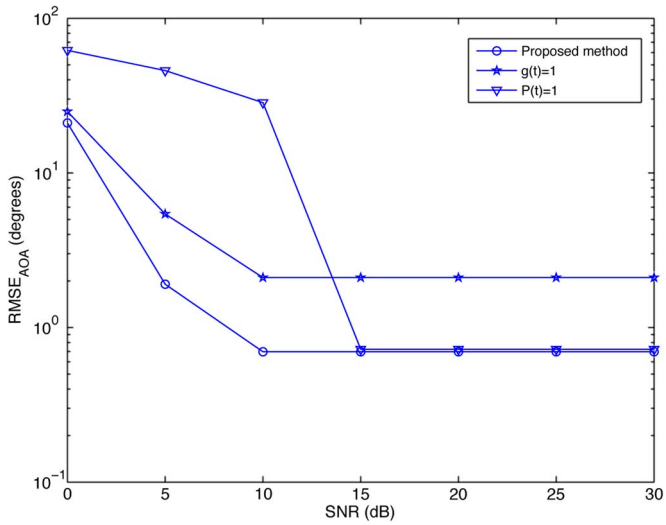

Fig. 7. RMSE of AOA estimates versus SNR for different weighting ($Q = 4$).

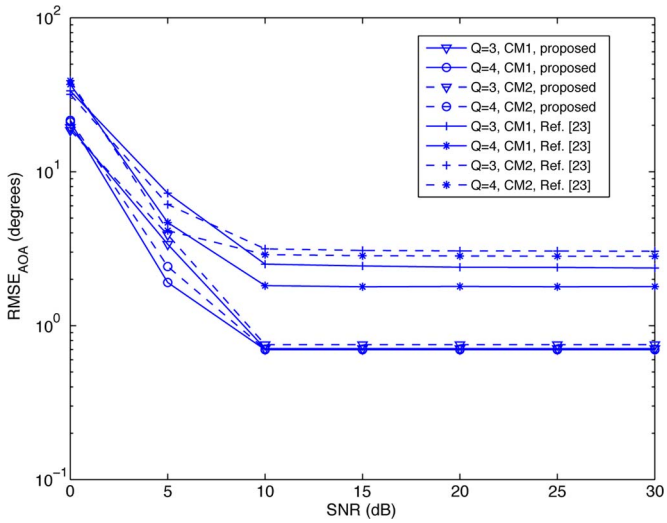

Fig. 8. RMSE of AOA estimates for both LOS (CM1) and NLOS (CM2) channels.

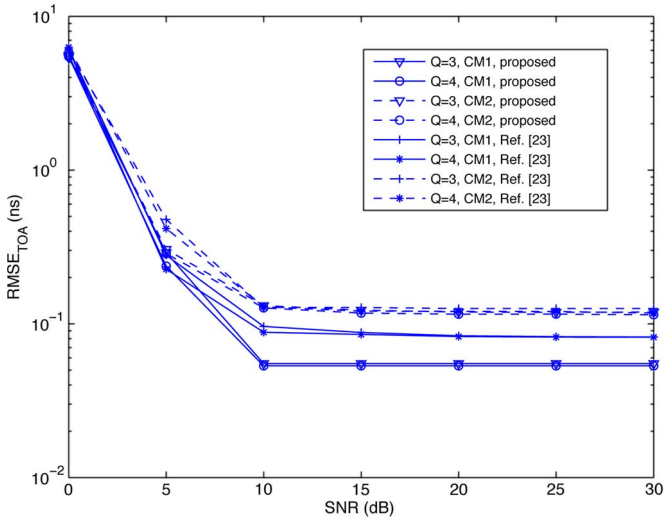

Fig. 9. RMSE of TOA estimates for both LOS (CM1) and NLOS (CM2) channels.

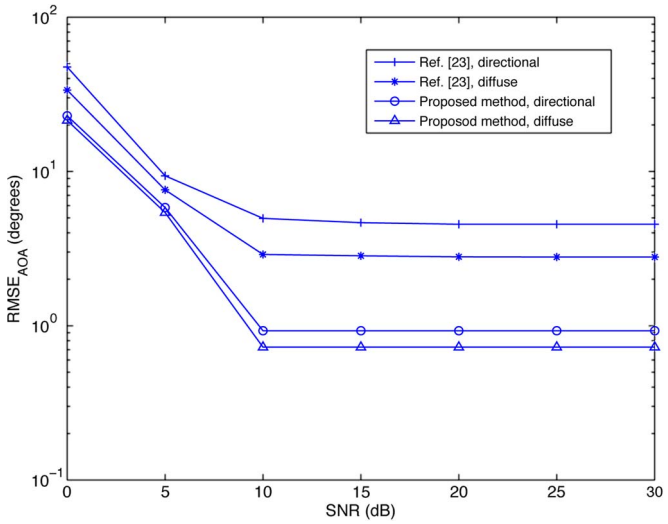

Fig. 10. RMSE of AOA estimates versus SNR for directional and diffuse secondary image fields ($Q = 2$).

the estimation performance of (23) with two other estimators derived from it as follows: (i) by setting $g(t - \tau_q) = 1,\ \forall\, t$, and keeping $P(t)$; and (ii) by setting $P(t) = 1,\ \forall\, t$, and keeping $g(t - \tau_q)$. According to these results, both the gating function and the APDP are necessary for the proposed estimator to achieve its best performance; that is, neglecting either one of them will cause an obvious performance degradation.

To verify the performance of the proposed estimator in non-line-of-sight (NLOS) conditions, we also considered the case of residential NLOS channels (CM2) in the IEEE 802.15.4a standard. In Figs. 8 and 9, we show the AOA and TOA estimation performance, respectively, of the proposed method as well as of the method in [23] for ULAs with $Q = 3$ and 4 antennas. For reference, we also include the performance of these estimators for the LOS IEEE 802.15.4a channel models (CM1). It is clear that even under NLOS conditions, the proposed estimator remains competitive and outperforms the reference method.

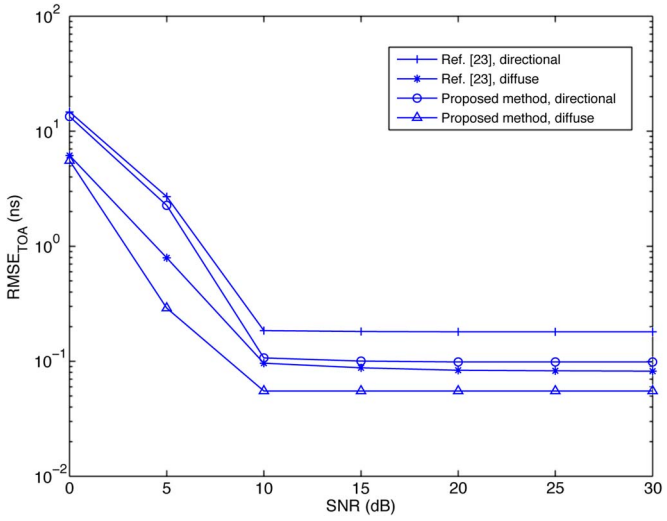

Fig. 11. RMSE of TOA estimates versus SNR for directional and diffuse secondary image fields ($Q = 2$).

C. Directional Image Field

A limiting case of interest is that of a highly directional image field, in which all the paths are arriving almost from the same angle within a very narrow aperture. This could be the case in a LOS environment, where the emitting source is surrounded by multiple reflecting objects in its immediate vicinity. In our simulations, to emulate this configuration, we simply set the mean angle of each cluster to the same value, i.e., 60°. As before, the AOA of each path follows a Laplacian distribution with standard deviation of 5°.

Fig. 10 shows the performance of both the proposed method and the one in [23] under this special condition of propagation. Comparing these results with those for the diffuse image field, we note that the AOA estimation accuracy of both methods is degraded. This is due to the fact that it is now more difficult to exploit the spatial information to separate the primary image path from the secondary ones. Nevertheless, in this more challenging scenario, the proposed estimator still outperforms the one in [23]. Similar conclusion can be drawn for the results of TOA estimation shown in Fig. 11.

VII. Conclusion

In this paper, we proposed a novel joint TOA and AOA estimator for dense multipath UWB environments. The proposed method consists of two steps: (1) preliminary estimation of the TOA and *a priori* information; (2) joint estimation of the TOA and AOA by maximization of a new LLF which employs the preliminary estimates from the first step. The derivation of this LLF relies on a special formulation in which the superposition of pulse images from the secondary paths is modeled as a Gaussian random process being characterized by a wideband space–time correlation function which uses a gating mechanism to represent the onset of the secondary paths and also takes into account the APDP.

In simulations based on multipath UWB channel models, our approach exhibits superior performance to that of a

competing scheme from the recent literature. For a typical UWB environment based on the standard CM1 channel model and diffuse image field, with 2 antennas spaced 50 cm apart, a SNR of 10 dB and a sampling rate of 16 GHz, the proposed joint estimator can provide an angular accuracy around 0.7° and a timing accuracy of less than 0.1 ns (corresponding to 3 cm in range). Furthermore, the estimation accuracy improves with finer interpolation of the LLF as well as by increasing the number of antennas. The proposed estimator was also tested in an extreme case of highly directional image field, as well as in the case of NLOS channels; in both cases, the obtained estimation accuracy remains competitive both for TOA and AOA parameters.

In future work, a more sophisticated spatial model could be developed that more accurately represents the directional image fields encountered in practical applications. To be specific, this can be done by modifying the space–time correlation function in (5), and especially the spatial component $\varrho(q, q')$. Currently, there is no clear description for the space–time correlation of the channel response at different antenna elements, especially for the extreme case of a very directional image field. It is therefore worthwhile to develop new functional relations which can embody the characteristics of such highly directional paths.

APPENDIX A

First, we focus on the diagonal entries. Starting with J_{11} and using "prime" to denote differentiation w.r.t. time t, as in e.g., $\eta'(t) = \partial\eta(t)/\partial t$, we have

$$\frac{\partial \ln \Lambda(\mathbf{x};\boldsymbol{\phi})}{\partial \tau} = -\frac{T_s}{2}\sum_{q=0}^{Q-1}\sum_{t\in\mathcal{T}}\left[\frac{2\sqrt{E_p}y_q(t)\eta'(t-\tau_q)}{\gamma(t,\tau_q)} - \left(\frac{y_q(t)^2}{\gamma(t,\tau_q)^2} - \frac{1}{\gamma(t,\tau_q)}\right)\frac{\partial\gamma(t,\tau_q)}{\partial\tau}\right] \quad (45)$$

where

$$\gamma(t,\tau_q) = E_p g(t-\tau_q)P(t) + \sigma_{\tilde{n}}^2 \quad (46)$$

$$y_q(t) = x_q(t) - \sqrt{E_p}\eta(t-\tau_q) \quad (47)$$

and

$$\frac{\partial\gamma(t,\tau_q)}{\partial\tau} = -E_p g'(t-\tau_q)P(t). \quad (48)$$

Taking the derivative of (45), and applying the expectation operation, we can write J_{11} as

$$J_{11} = -E\left[\frac{\partial^2 \ln\Lambda(\mathbf{x};\boldsymbol{\phi})}{\partial^2\tau}\right] = \sum_{q=0}^{Q-1} S_q \quad (49)$$

where we define

$$S_q = \sum_{t\in\mathcal{T}}\left[\frac{E_p\eta'(t-\tau_q)^2}{\gamma(t,\tau_q)} + \frac{1}{2\gamma(t,\tau_q)^2}\left(\frac{\partial\gamma(t,\tau_q)}{\partial\tau}\right)^2\right]T_s. \quad (50)$$

To obtain (49) we used the fact that, according to the channel model described in Section II, we have

$$E\left[y_q(t)\right] = 0 \quad (51)$$

and

$$E\left[y_q(t)^2\right] = \gamma(t,\tau_q). \quad (52)$$

Due to the slowly varying nature of the APDP and the fact that no signal power is received at the very beginning and end of a symbol interval, it follows that, in practice, S_q does not vary appreciably with the antenna index. That is, $S_q \approx S$ for all q. Therefore, we can write

$$J_{11} = SQ. \quad (53)$$

Performing similar calculations for J_{22}, we then get

$$J_{22} = -E\left[\frac{\partial^2\ln\Lambda(\mathbf{x};\boldsymbol{\phi})}{\partial^2\theta}\right] \quad (54)$$

$$= S\sum_{q=0}^{Q-1}\left(\frac{\partial\tau_q}{\partial\theta}\right)^2 = S\frac{d^2}{c^2}(\sin\theta)^2\Psi \quad (55)$$

where the last equalities in (55) follow from (2), and the constant Ψ is defined as $\Psi = Q(Q-1)(Q+1)/12$.

For J_{33}, using the general term $\boldsymbol{\phi}_\eta$, the first derivative is

$$\frac{\partial\ln\Lambda(\mathbf{x};\boldsymbol{\phi})}{\partial\boldsymbol{\phi}_\eta} = T_s\sum_{q=0}^{Q-1}\sum_{t\in\mathcal{T}}\frac{\sqrt{E_p}y_q(t)}{\gamma(t,\tau_q)}\frac{\partial\eta(t-\tau_q)}{\partial\boldsymbol{\phi}_\eta} \quad (56)$$

and therefore

$$J_{33} = -E\left[\frac{\partial^2\ln\Lambda(\mathbf{x};\boldsymbol{\phi})}{\partial^2\boldsymbol{\phi}_\eta}\right] \quad (57)$$

$$= T_s\sum_{q=0}^{Q-1}\sum_{t\in\mathcal{T}}\frac{E_p}{\gamma(t,\tau_q)}\left(\frac{\partial\eta(t-\tau_q)}{\partial\boldsymbol{\phi}_\eta}\right)^2. \quad (58)$$

For J_{44}, we use the general term $\boldsymbol{\phi}_\zeta$. The first derivative becomes

$$\frac{\partial\ln\Lambda(\mathbf{x};\boldsymbol{\phi})}{\partial\boldsymbol{\phi}_\zeta} = \frac{T_s}{2}\sum_{q=0}^{Q-1}\sum_{t\in\mathcal{T}}\left[\frac{y_q^2(t)}{\gamma^2(t,\tau_q)} - \frac{1}{\gamma(t,\tau_q)}\right]\frac{\partial\gamma(t,\tau_q)}{\partial\boldsymbol{\phi}_\zeta} \quad (59)$$

and

$$J_{44} = -E\left[\frac{\partial^2\ln\Lambda(\mathbf{x};\boldsymbol{\phi})}{\partial^2\boldsymbol{\phi}_\zeta}\right] \quad (60)$$

$$= \frac{T_s}{2}\sum_{q=0}^{Q-1}\sum_{t\in\mathcal{T}}\frac{1}{\gamma^2(t,\tau_q)}\left(\frac{\partial\gamma(t,\tau_q)}{\partial\boldsymbol{\phi}_\zeta}\right)^2. \quad (61)$$

The rest of the entries of the FIM are the cross terms. In particular, due to the array geometry, we have that

$$J_{12} = J_{21} = -E\left[\frac{\partial^2\ln\Lambda(\mathbf{x};\boldsymbol{\phi})}{\partial\tau\partial\theta}\right] \quad (62)$$

$$= S \sum_{q=0}^{Q-1} \frac{\partial \tau_q}{\partial \theta} = 0. \tag{63}$$

In addition,

$$J_{13} = J_{31} = -E\left[\frac{\partial^2 \ln \Lambda(\mathbf{x};\boldsymbol{\phi})}{\partial \tau \partial \boldsymbol{\phi}_\eta}\right] \tag{64}$$

$$= -\sum_{q=0}^{Q-1} S_q^{13} \tag{65}$$

where

$$S_q^{13} = \sum_{t\in\mathcal{T}} T_s E_p \frac{\eta'(t-\tau_q)}{\gamma(t,\tau_q)} \frac{\partial \eta(t-\tau_q)}{\partial \boldsymbol{\phi}_\eta} \tag{66}$$

and

$$J_{14} = J_{41} = -E\left[\frac{\partial^2 \ln \Lambda(\mathbf{x};\boldsymbol{\phi})}{\partial \tau \partial \boldsymbol{\phi}_\zeta}\right] \tag{67}$$

$$= \sum_{q=0}^{Q-1} S_q^{14} \tag{68}$$

where

$$S_q^{14} = \frac{T_s}{2} \sum_{t\in\mathcal{T}} \frac{1}{\gamma^2(t,\tau_q)} \frac{\partial \gamma(t,\tau_q)}{\partial \boldsymbol{\phi}_\zeta} \frac{\partial \gamma(t,\tau_q)}{\partial \tau}. \tag{69}$$

Similarly to S_q, in practice, S_q^{13} and S_q^{14} do not vary appreciably with the antenna index and therefore we let $S^{13} = S_q^{13}$ and $S^{14} = S_q^{14}$, for all q. Consequently, we can write $J_{13} = J_{31} = QS^{13}$, $J_{14} = J_{41} = QS^{14}$ and

$$J_{24} = J_{42} = -E\left[\frac{\partial^2 \ln \Lambda(\mathbf{x};\boldsymbol{\phi})}{\partial \theta \partial \boldsymbol{\phi}_\zeta}\right] \tag{70}$$

$$= S^{14} \sum_{q=0}^{Q-1} \frac{\partial \tau_q}{\partial \theta} = 0. \tag{71}$$

Finally, it is also not difficult to prove that

$$J_{23} = J_{32} = J_{34} = J_{43} = 0. \tag{72}$$

Consequently, the matrices $\boldsymbol{A}$, $\boldsymbol{B}$, and $\boldsymbol{C}$ can be written as

$$\boldsymbol{A} = \begin{bmatrix} J_{11} & 0 \\ 0 & J_{22} \end{bmatrix} \tag{73}$$

$$\boldsymbol{B} = \begin{bmatrix} J_{33} & 0 \\ 0 & J_{44} \end{bmatrix} \tag{74}$$

$$\boldsymbol{C} = \begin{bmatrix} J_{13} & J_{14} \\ 0 & 0 \end{bmatrix} \tag{75}$$

and therefore the EFIM is

$$\boldsymbol{A} - \boldsymbol{C}\boldsymbol{B}^{-1}\boldsymbol{C}^T = \begin{bmatrix} J_{11} - J_{13}J_{33}^{-1}J_{31} - J_{14}J_{44}^{-1}J_{41} & 0 \\ 0 & J_{22} \end{bmatrix}. \tag{76}$$

REFERENCES

[1] D. Dardari, R. D'Errico, C. Roblin, A. Sibille, and M. Win, "Ultrawide bandwidth RFID: The next generation?" *Proc. IEEE*, vol. 98, no. 9, pp. 1570–1582, Sep. 2010.

[2] M. Win *et al.*, "Network localization and navigation via cooperation," *IEEE Commun. Mag.*, vol. 49, no. 5, pp. 56–62, May 2011.

[3] Y. Shen and M. Win, "Fundamental limits of wideband localization—Part I: A general framework," *IEEE Trans. Inf. Theory*, vol. 56, no. 10, pp. 4956–4980, Oct. 2010.

[4] A. Conti, M. Guerra, D. Dardari, N. Decarli, and M. Win, "Network experimentation for cooperative localization," *IEEE J. Sel. Areas Commun.*, vol. 30, no. 2, pp. 467–475, Feb. 2012.

[5] A. Conti, D. Dardari, M. Guerra, L. Mucchi, and M. Z. Win, "Experimental characterization of diversity navigation," *IEEE Syst. J.*, vol. 8, no. 1, pp. 115–124, Mar. 2014.

[6] B. Alavi and K. Pahlavan, "Modeling of the TOA-based distance measurement error using UWB indoor radio measurements," *IEEE Commun. Lett.*, vol. 10, no. 4, pp. 275–277, Apr. 2006.

[7] Z. Sahinoglu, S. Gezici, and I. Gvenc, *Ultra-Wideband Positioning Systems: Theoretical Limits, Ranging Algorithms, and Protocols*. Cambridge, U.K.: Cambridge Univ. Press, 2008.

[8] D. Dardari, A. Conti, U. Ferner, A. Giorgetti, and M. Win, "Ranging with ultrawide bandwidth signals in multipath environments," *Proc. IEEE*, vol. 97, no. 2, pp. 404–426, Feb. 2009.

[9] J. Y. Lee and R. Scholtz, "Ranging in a dense multipath environment using an UWB radio link," *IEEE J. Sel. Areas Commun.*, vol. 20, no. 9, pp. 1677–1683, Dec. 2002.

[10] M. Win and R. Scholtz, "Characterization of ultra-wide bandwidth wireless indoor channels: A communication-theoretic view," *IEEE J. Sel. Areas Commun.*, vol. 20, no. 9, pp. 1613–1627, Dec. 2002.

[11] W. Liu, H. Ding, X. Huang, and Z. Liu, "TOA estimation in IR UWB ranging with energy detection receiver using received signal characteristics," *IEEE Commun. Lett.*, vol. 16, no. 5, pp. 738–741, May 2012.

[12] I. Guvenc and Z. Sahinoglu, "Threshold selection for UWB TOA estimation based on kurtosis analysis," *IEEE Commun. Lett.*, vol. 9, no. 12, pp. 1025–1027, Dec. 2005.

[13] J. Youssef, B. Denis, C. Godin, and S. Lesecq, "New TOA estimators within energy-based receivers under realistic UWB channel statistics," in *Proc. IEEE Veh. Tech. Conf.*, May 2010, pp. 1–5.

[14] Y. Chen and N. Beaulieu, "New receiver designs for generalized UWB transmitted reference systems," in *Proc. IEEE Int. Conf. Commun.*, May 2008, pp. 3923–3927.

[15] I. Guvenc, S. Gezici, and Z. Sahinoglu, "Ultra-wideband range estimation: Theoretical limits and practical algorithms," in *Proc. IEEE Int. Conf. Ultra-Wideband*, Sep. 2008, vol. 3, pp. 93–96.

[16] F. Shang, B. Champagne, and I. Psaromiligkos, "Joint estimation of time of arrival and channel power delay profile for pulse-based UWB systems," in *Proc. IEEE Int. Conf. Commun.*, Jun. 2012, pp. 4515–4519.

[17] F. Shang, B. Champagne, and I. Psaromiligkos, "Time of arrival and power delay profile estimation for IR-UWB systems," *Signal Process.*, vol. 93, no. 5, pp. 1317–1327, May 2013.

[18] Y. Shen and M. Z. Win, "On the accuracy of localization systems using wideband antenna arrays," *IEEE Trans. Commun.*, vol. 58, no. 1, pp. 270–280, Jan. 2010.

[19] H. S. Lee and C. Sodini, "Analog-to-digital converters: Digitizing the analog world," *Proc. IEEE*, vol. 96, no. 2, pp. 323–334, Feb. 2008.

[20] H. Keshavarz, "Weighted signal-subspace direction-finding of ultra-wideband sources," in *Proc. IEEE Int. Conf. Wireless Mobile Comput., Netw. Commun.*, Aug. 2005, pp. 23–29.

[21] V. Mani and R. Bose, "Direction of arrival estimation and beamforming of multiple coherent UWB signals," in *Proc. IEEE Int. Conf. Commun.*, May 2010, pp. 1–5.

[22] Y. Luo and C. Law, "Indoor positioning using UWB-IR signals in the presence of dense multipath with path overlapping," *IEEE Trans. Wireless Commun.*, vol. 11, no. 10, pp. 3734–3743, Oct. 2012.

[23] L. Taponecco, A. A. D'Amico, and U. Mengali, "Joint TOA and AOA estimation for UWB localization applications," *IEEE Trans. Wireless Commun.*, vol. 10, no. 7, pp. 2207–2217, Jul. 2011.

[24] E. Lagunas, M. Najar, and M. Navarro, "UWB joint TOA and DOA estimation," in *Proc. IEEE Int. Conf. Ultra-Wideband*, Sep. 2009, pp. 839–843.

[25] M. Navarro and M. Najar, "Frequency domain joint TOA and DOA estimation in IR-UWB," *IEEE Trans. Wireless Commun.*, vol. 10, no. 10, pp. 1–11, Oct. 2011.

[26] F. Shang, B. Champagne, and I. Psaromiligkos, "A novel ML based joint TOA and AOA estimator for IR-UWB systems," in *Proc. IEEE Int. Conf. Acoust., Speech, Signal Process.*, May 2013, pp. 5190–5194.
[27] T. Santos, F. Tufvesson, and A. Molisch, "Modeling the ultra-wideband outdoor channel: Model specification and validation," *IEEE Trans. Wireless Commun.*, vol. 9, no. 6, pp. 1987–1997, Jun. 2010.
[28] P. Meissner and K. Witrisal, "Analysis of position-related information in measured UWB indoor channels," in *Proc. 6th Eur. Conf. Antennas Propag.*, 2012, pp. 6–10.
[29] Z. Sahinoglu and S. Gezici, "Ranging in the IEEE 802.15.4a standard," in *Proc. IEEE Wireless Microw. Tech.Conf.*, Dec. 2006, pp. 1–5.
[30] U. Schuster and H. Bolcskei, "Ultrawideband channel modeling on the basis of information-theoretic criteria," *IEEE Trans. Wireless Commun.*, vol. 6, no. 7, pp. 2464–2475, Jul. 2007.
[31] H. Luecken, C. Steiner, and A. Wittneben, "ML timing estimation for generalized UWB-IR energy detection receivers," in *Proc. IEEE Int. Conf. Ultra Wideband*, Sep. 2009, pp. 829–833.
[32] K. Makaratat, T. Brown, and S. Stavrou, "Estimation of time of arrival of UWB multipath clusters through a spatial correlation technique," *IET Microw. Antennas Propag.*, vol. 1, no. 3, pp. 666–673, Jun. 2007.
[33] G. Durgin and T. Rappaport, "Effects of multipath angular spread on the spatial cross-correlation of received voltage envelopes," in *Proc. IEEE Veh. Technol. Conf.*, Jun. 1999, pp. 996–1000.
[34] A. F. Molisch, "Ultra-wide-band propagation channel," *Proc. IEEE*, vol. 97, no. 2, pp. 353–371, Feb. 2009.
[35] H. Chaibi, R. Saadane, M. A. Fagihi, and M. Belkasmi, "Spatial correlation characterization for UWB indoor channel based on measurements," in *Proc. Int. Conf. Image Signal Process.*, 2012, pp. 149–156.
[36] D. M. Cassioli, M. Win, and A. Molisch, "The ultra-wide bandwidth indoor channel: From statistical model to simulations," *IEEE J. Sel. Areas Commun.*, vol. 20, no. 6, pp. 1247–1257, Aug. 2002.
[37] F. C. Schweppe, "Evaluation of likelihood functions for Gaussian signals," *IEEE Trans. Inf. Theory*, vol. IT-11, no. 1, pp. 61–70, Jan. 1965.
[38] A. Mallat, J. Louveaux, and L. Vandendorpe, "UWB based positioning in multipath channels: CRBs for AOA and for hybrid TOA-AOA based methods," in *Proc. IEEE Int. Conf. Commun.*, Jun. 2007, pp. 5775–5780.
[39] D. Dardari, C. Chong, and M. Win, "Threshold-based time-of-arrival estimators in UWB dense multipath channels," *IEEE Trans. Commun.*, vol. 56, no. 8, pp. 1366–1378, Aug. 2008.
[40] A. Molisch *et al.*, "IEEE 802.15.4a channel model—Final report," IEEE 802.15 WPAN Low Rate Alternative PHY Task Group 4a (TG4a), Nov. 2004.
[41] R.-M. Cramer, R. Scholtz, and M. Win, "Evaluation of an ultra-wideband propagation channel," *IEEE Trans. Antennas Propag.*, vol. 50, no. 5, pp. 561–570, May 2002.
[42] S. Venkatesh, V. Bharadwaj, and R. Buehrer, "A new spatial model for impulse-based ultra-wideband channels," in *Proc. IEEE Veh. Technol. Conf.*, Sep. 2005, pp. 2617–2621.
[43] S. Gezici *et al.*, "Localization via ultra-wideband radios: A look at positioning aspects for future sensor networks," *IEEE Signal Process. Mag.*, vol. 22, no. 4, pp. 70–84, Jul. 2005.

Fang Shang received the B.Sc. and M.Eng. degrees from Central South University, Hunan, China, in 2005 and 2007, respectively, and the Ph.D. degree in electrical engineering from McGill University, Montreal, QC, USA, in 2014. Her main research interests are in the field of IR-UWB technology, channel modeling, parameter estimation, and UWB systems for location and tracking.

Benoit Champagne (S'87–M'89–SM'03) received the B.Ing. degree in engineering physics from the École Polytechnique de Montréal, Montreal, QC, Canada, in 1983, the M.Sc. degree in physics from the Université de Montréal, Montreal, in 1985, and the Ph.D. degree in electrical engineering from the University of Toronto, Toronto, ON, Canada, in 1990. From 1990 to 1999, he was an Assistant Professor and then an Associate Professor at INRS-Telecommunications, Université du Québec, Montreal. In 1999, he joined McGill University, Montreal, where he is now a Full Professor within the Department of Electrical and Computer Engineering. He served as an Associate Chairman of Graduate Studies in the Department from 2004 to 2007. His research focuses on the study of advanced algorithms for the processing of information bearing signals by digital means. His interests span many areas of statistical signal processing, including detection and estimation, sensor array processing, adaptive filtering, and applications thereof to broadband communications and audio processing, where he has co-authored more than 200 referred publications. His research has been funded by the Natural Sciences and Engineering Research Council of Canada, the "Fonds de Recherche sur la Nature et les Technologies" from the Government of Quebec, as well as some major industrial sponsors, including Nortel Networks, Bell Canada, InterDigital, and Microsemi. Prof. Champagne has been an Associate Editor of the IEEE SIGNAL PROCESSING LETTERS, IEEE TRANSACTIONS ON SIGNAL PROCESSING, and *EURASIP Journal on Applied Signal Processing*. He has also served on the Technical Committees of several international conferences in the fields of communications and signal processing. In particular, he was Co-Chair, Wide Area Cellular Communications Track, for the IEEE Int. Symp. on PIMRC (Toronto, Sept. 2011); Co-Chair, Antenna and Propagation Track, for the IEEE VTC-Fall (Los Angeles, CA, USA, Sept. 2004); and Registration Chair, for the IEEE Int. Conf. on ASSP (Montreal, May 2004).

Ioannis N. Psaromiligkos (S'96–M'03) received the Diploma degree in computer engineering and science from the University of Patras, Patras, Greece, in 1995 and the M.S. and Ph.D. degrees in electrical engineering from the State University of New York at Buffalo, NY, USA, in 1997 and 2001, respectively. Since 2001, he has been with the Department of Electrical and Computer Engineering, McGill University, Montreal, QC, Canada, where he is currently an Associate Professor. His research interests are in the areas of statistical detection and estimation, adaptive signal processing, machine learning, and wireless communications.

Dr. Psaromiligkos has served as an Associate Editor of the IEEE COMMUNICATIONS LETTERS and IEEE SIGNAL PROCESSING LETTERS and is currently an Associate Editor of the *EURASIP Journal on Advances in Signal Processing*.